Bulletin of the Earthquake
Research Institute
Vol. 42 (1964), pp. 273-287

15. *Propagation of Spheroidal Disturbances on a Homogeneous Elastic Sphere.*

By Tatsuo Usami and Yasuo Satô,*

Earthquake Research Institute.

(Read March 24, 1964.—Received March 31, 1964.)

Abstract

Theoretical seismograms of radial and colatitudinal displacement were calculated on the surface of a homogeneous elastic sphere for a transient stress acting on a small area around the pole. The axial symmetry was assumed and the disturbances were expressed as the sum of contribution of about 600 normal mode oscillations.

The theoretical seismograms thus obtained show the following remarkable features.

1) The arrival times of body waves identified on the theoretical seismogram coincide well with the theoretically calculated travel time.

2) The fundamental mode contributes to the surface waves most, while the higher modes are closely connected with the phases of body waves.

3) Surface waves end abruptly and a calm follows, which fact can be inferred from the shape of the group velocity curve with a minimum value.

Non-dimensional frequency, phase and group velocities of surface wave, common spectrum as a function of n and the travel time curve of various phases are also given in the figures.

1. Introduction

A few years ago propagation of torsional disturbances on the surface of an elastic sphere was studied and theoretical seismograms for a localized force acting around the pole were calculated.[1] From this study, in which various normal modes of free torsional oscillations were super-

* This work was started when T. Usami was at Lamont Geological Observatory, Columbia University, New York, on leave from the Japan Meteorological Agency and Y. Satô was at Watson Research Laboratory, IBM, New York, on leave from the Earthquake Research Institute, the University of Tokyo. (Lamont Geological Observatory Contribution No. 721)

posed, it was made clear how body waves as well as surface waves are propagated on the surface of a sphere.

In the present paper, however, a uniform pressure is assumed on a small circular area around the pole and the problem of the propagation of disturbances is studied by the superposition of the spheroidal free oscillations.

2. Fundamental expressions

We assume that:

1) The sphere is homogeneous.

2) The dilatational and second kind rotational waves are employed.

3) The radial component of stress is applied on a localized area around the pole.

4) The effect of gravity is neglected.

The boundary conditions to be satisfied at the surface $r=a$ are

$$\begin{aligned}&\widehat{rr}=\Phi(\theta,\varphi)\cdot f(t)=\{\sum_{m,n}(\Phi_{mn}\cos m\varphi+\Phi'_{mn}\sin m\varphi)\}\cdot f(t)\ ,\\&\widehat{r\theta}=0\ ,\\&\widehat{r\varphi}=0\ .\end{aligned}\tag{2.1}$$

The displacement on the surface is expressed as

$$(u,v,w)=\frac{1}{2\pi}\int_{-\infty}^{\infty}(u(p),v(p),w(p))\cdot\exp(jpt)\,dp\ ,\tag{2.2}$$

in which

$$\begin{aligned}u(p)&=\sum_{m,n}(U_n(r)/E)\cdot P_n^m(\cos\theta)\cdot(C_{mn}\cos m\varphi+C'_{mn}\sin m\varphi)\cdot f^*(p)\ ,\\v(p)&=\sum_{m,n}(V_n(r)/E)\cdot\frac{d}{d\theta}P_n^m(\cos\theta)\cdot(C_{mn}\cos m\varphi+C'_{mn}\sin m\varphi)\cdot f^*(p)\ ,\\w(p)&=\sum_{m,n}m(V_n(r)/E)\cdot\frac{P_n^m(\cos\theta)}{\sin\theta}\cdot(-C_{mn}\sin m\varphi+C'_{mn}\cos m\varphi)\cdot f^*(p)\ ,\end{aligned}\tag{2.3}$$

and

$$\begin{aligned}E=&-\mu\left(\lambda h^2 f_n-2\mu\frac{d^2}{da^2}f_n\right)\left(\frac{d^2}{da^2}g_n+(n(n+1)-2)\frac{g_n}{a^2}\right)\\&-4\mu^2 n(n+1)\frac{d}{da}\left(\frac{f_n}{a}\right)\cdot\frac{d}{da}\left(\frac{g_n}{a}\right)\ ,\\f_n=&J_{n+1/2}(ha)/\sqrt{ha}\ ,\qquad h=p/V_p\ ,\\g_n=&J_{n+1/2}(ka)/\sqrt{ka}\ ,\qquad k=p/V_s\ ,\end{aligned}\tag{2.4}$$

$$\left.\begin{matrix} C_{mn} \\ C'_{mn} \end{matrix}\right\} = K_n^m \int_{-1}^{1} \left\{\begin{matrix} \Phi_{mn} \\ \Phi'_{mn} \end{matrix}\right\} \cdot P_n^m(\cos\theta) \cdot d(\cos\theta) ,$$

$$K_n^m = \frac{2n+1}{2\pi} \cdot \delta_m \cdot \frac{(n-m)!}{(n+m)!} , \qquad \delta_m = \begin{cases} 1 & m \neq 0 \\ 1/2 & m = 0 \end{cases} , \tag{2.5}$$

$f^*(p)$=Fourier transform of the function $f(t)$,

j=unit of imaginary number ,

$$U_n(r) = -\mu \frac{d}{da} f_n \cdot \left[k^2 g_n + 2 \frac{d}{da}\left(\frac{1}{a} \frac{d}{da}(a g_n) \right) \right] + 2\mu n(n+1) \frac{g_n}{a} \cdot \frac{d}{da}\left(\frac{f_n}{a} \right) ,$$

$$V_n(r) = -\mu \frac{f_n}{a} \cdot \left[k^2 g_n + 2 \frac{d}{da}\left(\frac{1}{a} \frac{d}{da}(a g_n) \right) \right] + \frac{2\mu}{a} \frac{d}{da}(a g_n) \cdot \frac{d}{da}\left(\frac{f_n}{a} \right) . \tag{2.6}$$

$E=0$ is the frequency equation for the spheroidal oscillation of a homogeneous elastic sphere.

The integral is evaluated by the method of contour integration and is given by

$$\begin{aligned} u &= \frac{1}{2\pi} \sum_{m,n} P_n^m(\cos\theta) \cdot (C_{mn} \cos m\varphi + C'_{mn} \sin m\varphi) \\ &\quad \cdot \int_{-\infty}^{\infty} \frac{U_n(r)}{E} f^*(p) \cdot \exp(jpt) dp , \\ &= \frac{j}{2} \sum_{m,n,i} P_n^m(\cos\theta) \cdot (C_{mn} \cos m\varphi + C'_{mn} \sin m\varphi) \\ &\quad \cdot \left[\frac{U_n(r)}{dE/dp} \cdot f^*(p) \cdot \exp(jpt) \right]_{p={}_i p_n} , \end{aligned} \tag{2.7}$$

where ${}_i p_n$ is the root of frequency equation $E=0$ and i is the radial mode number. As to the expressions for v and w, similar formulas can easily be obtained.

In actual computation, we confine ourselves to the case of axial symmetry ($m=0$), consequently the azimuthal displacement w is identically zero, and $\lambda=\mu$ is assumed.

3. Non-dimensional frequency of the spheroidal oscillation of a homogeneous elastic sphere

The non-dimensional frequency ka for $i=1\sim5$, $n>60$ and for $i=6\sim9$, $n\geqq0$, were added to our previous results[2] in order to give better

accuracy to the theoretical seismograms and to make a detailed analysis possible. In Fig. 1 non-dimensional frequency is given in the form of

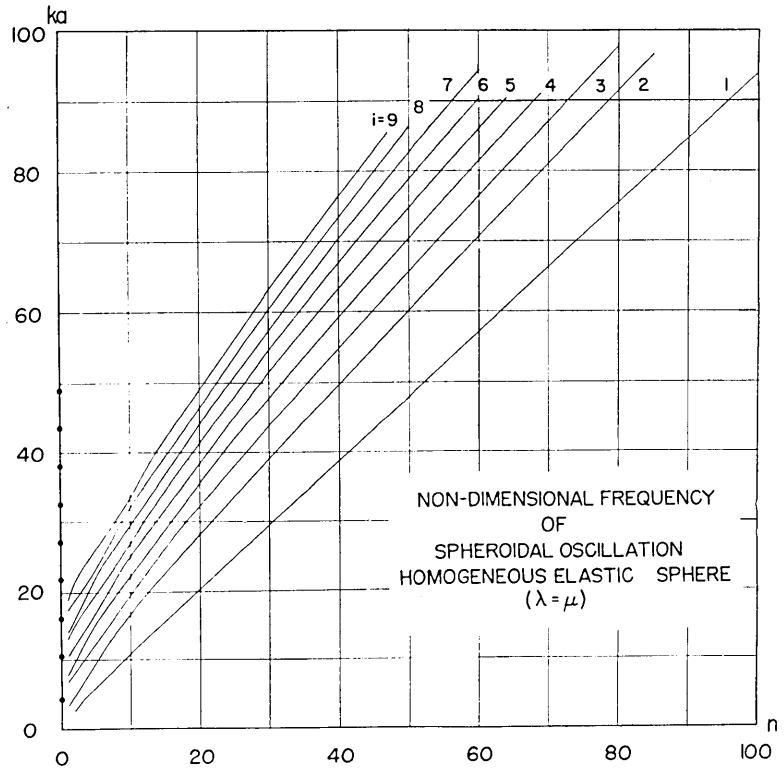

Fig. 1. Non-dimensional frequency ($ka=(2\pi a/V_s)/T$) of the spheroidal free oscillation of a homogeneous elastic sphere. Although discrete points for integer values of n are significant, points are connected by a curve for each value of radial mode number i, except those for $n=0$ which are shown by solid circles.

curves connecting points which belong to the same parameter value i. $n=0$ is the exceptional case, for which solid circles are given. The curves show undulation for higher modes at small values of n. The range of n showing this irregularity becomes larger as the radial mode number i increases. This irregularity has a direct relation with the appearance of minimum and maximum in the group velocity curve in Fig. 2.

4. Phase and group velocities

Wavelengths of the free oscillation of a sphere on the surface are calculated by the well-known asymptotic relation[3]

$$\text{wavelength}=(2\pi a)/(n+1/2)\ . \tag{4.1}$$

Though the formula holds only for large values of n, the same expression was tentatively applied to small values of n in the numerical computation of phase velocity. We have non-dimensional frequency

$$\eta=ka=(2\pi a/V_s)/T\ . \tag{4.2}$$

Combining (4.1) and (4.2)

$$\begin{aligned} C\ (&=\text{Phase velocity}=\text{wavelength}/T)\\ &=[(2\pi a)/(n+1/2)]\cdot[\eta/(2\pi a/V_s)]\ ,\\ C/V_s&=\eta/(n+1/2)\ . \end{aligned} \tag{4.3}$$

Group velocity U is also calculated by the following non-dimensional formula

$$U/V_s=d\eta/dn\ . \tag{4.4}$$

Calculated values of phase and group velocities are arranged in Fig. 2. There are remarkable differences between the cases of torsional[4] and spheroidal oscillations. In the former case both curves are very simple and the phase velocity decreases uniformly as the wavelength decreases, while in the spheroidal oscillation the phase velocity curve shows a rather peculiar change of slope. Another marked difference is the existence of minimum and maximum in the group velocity curve, a natural consequence of the irregularity in Fig. 1 for smaller values of n. Lastly, it must be noted that, for the fundamental mode ($i=1$), both phase and group velocities approach the velocity of Rayleigh wave in a homogeneous semi-infinite elastic medium, namely $C/V_s=0.9194$.

5. Common spectrum

In the equation (2.7), the expression for radial displacement, the coefficient of $P_n^m(\cos\theta)\cdot\cos m\varphi\cdot\exp(jpt)$ is considered as the common spectrum of disturbance. Assuming $m=0$, which is the actual case of our study, the common spectrum is expressed as the product of three

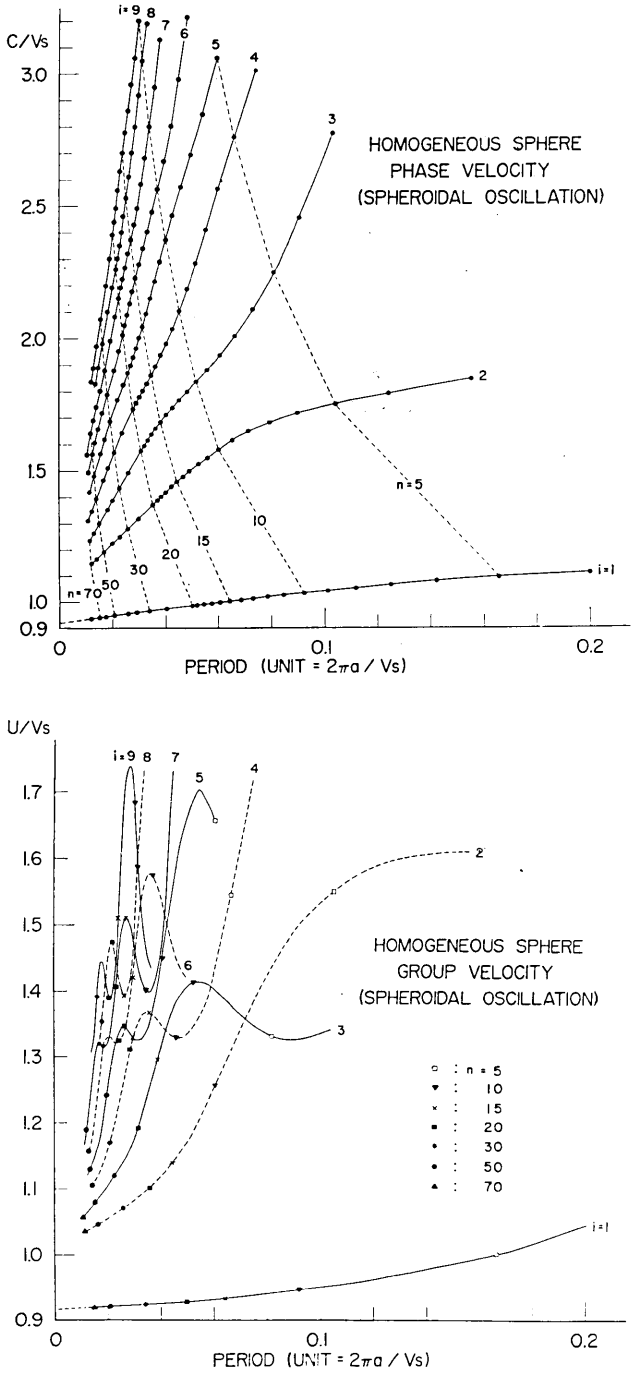

Fig. 2. Relation of phase and group velocities to period.

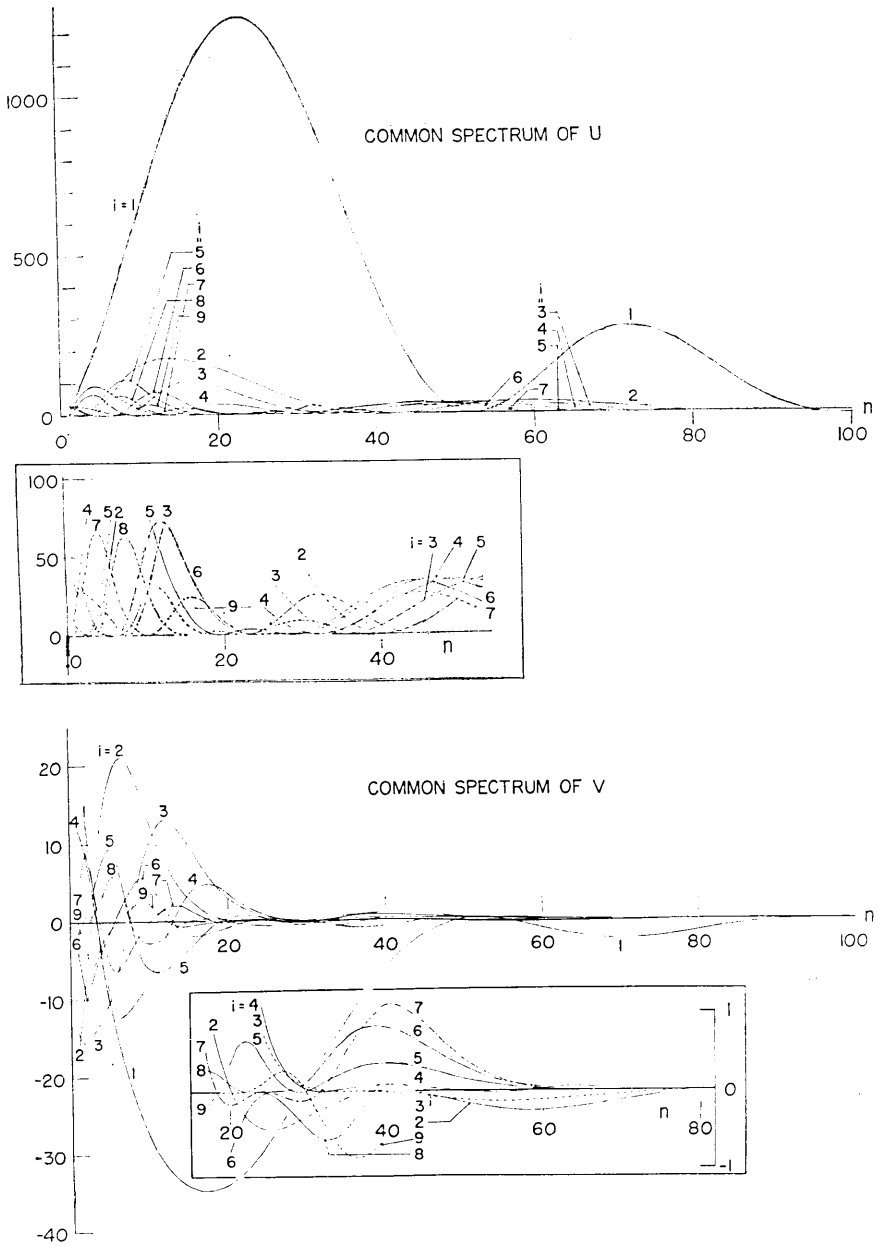

Fig. 3. Common spectrum of radial and colatitudinal components of disturbances. To show the features of curves clearly, a part of the figure is enlarged and is given in a rectangular enclosure. Circles on the line $n=0$ for the radial common spectrum correspond to the circles in Fig. 1 in the same order. (Amplitude in an arbitrary scale.)

factors

$$ {}_iS_n^u = C_{mn} \cdot \frac{U_n(r)}{dE/dp} \cdot f^*(p) \ . \tag{5.1} $$

${}_iS_n^v$, the common spectrum for the displacement component v has a similar form of expression. Using this common spectrum u, v and w are expressed as follows.

$$ \begin{aligned} u &= \sum_{n,i} {}_iS_n^u \cdot P_n(\cos\theta) \cdot \exp(jpt) \ , \\ v &= \sum_{n,i} {}_iS_n^v \cdot \frac{d}{d\theta} P_n(\cos\theta) \cdot \exp(jpt) \ , \\ w &= 0 \ . \end{aligned} \tag{5.2} $$

The common spectra for u and v are plotted in Fig. 3. The spectral values of u-component for $n=0$ are given by solid circles, which correspond to the solid circles in Fig. 1. A part of the figure is shown on a magnified scale to show a detailed feature.

6. Disturbances calculated on the surface

In the following numerical computations, as stated before, $m=0$ is assumed. As to the space distribution of stress we assume

$$ \Phi(\theta, \varphi) = \Phi^0(\cos\theta) = \begin{cases} 1 & \theta < \theta_0 \\ 0 & \theta > \theta_0 \ , \end{cases} \tag{6.1} $$

and the time distribution of the stress is assumed as

$$ f(t) = \begin{cases} -1 & -t_1 < t < 0 \\ 1 & 0 < t < t_1 \\ 0 & |t| > t_1 \ . \end{cases} \tag{6.2} $$

From the function given above, we have immediately

$$ f^*(p) = -j4 \cdot \sin^2(pt_1/2)/p \ . \tag{6.3} $$

The numerical values assumed are:

$$ \begin{aligned} \theta_0 &= 0.04 \text{ radian} \ , \\ t_1 &= 0.02 \ . \end{aligned} \tag{6.4} $$

In the last expression the unit of time is assumed to be $(2\pi a)/V_s$. Largest values of colatitudinal order number n employed are, for each value of radial mode number i,

$$\begin{array}{lccccccccc} i= & 1 & 2 & 3 & 4 & 5 & 6 & 7 & 8 & 9 \\ n_c= & 100 & 79 & 73 & 69 & 64 & 60 & 60 & 39 & 44 \end{array} \tag{6.5}$$

Curves of common spectrum pass zeroes near these values of n_c, beyond which the values are very small and the contribution becomes negligible.

The calculated disturbances at three points $\theta=30°$, $90°$, $150°$ are shown in Fig. 4. In this figure solid line implies $({}_9u_{100})$ and $({}_9v_{100})$, and broken line gives $({}_1u_{100})$ and $({}_1v_{100})$. The parentheses mean:

$$\begin{aligned} ({}_iu_n) &= \sum_{i=1}^{i} \sum_{n=0}^{n} {}_iu_n \ , \\ ({}_iv_n) &= \sum_{i=1}^{i} \sum_{n=0}^{n} {}_iv_n \ . \end{aligned} \tag{6.6}$$

Expected arrivals of various phases of P, S and P–S converted waves calculated by the simple theory of geometrical optics are indicated by arrows in Fig. 4. Fig. 5 shows the travel time curve of these waves for an impulsive source at the pole. Since the source has, in the present case, spatial dimension and time duration, we have to refer to the cross mark on the lower left-hand side instead of the origin point. Dots in this figure represent the points at which certain phases begin or terminate. For example SP, SSP, and 3SP begin at epicentral distances $\theta=109.5°$, $219.0°$ and $328.5°$ respectively.

In Fig. 4, the difference between the solid and broken lines is small during the passage of surface waves, while a remarkable discrepancy is found in the phases of body waves between these two curves. Besides, the broken line deviates little from the zero line except during the passage of surface wave. This fact confirms, as stated in our previous paper[5], that the fundamental mode expresses the surface wave and the radial higher mode is closely connected to the body waves. From this viewpoint the significance of radial higher modes of surface waves is an interesting problem to explore. It is remarkable that, on the broken lines, surface waves end abruptly and a calm follows. This fact is inferred from the shape of the group velocity curve for the fundamental mode. Actually, surface waves end exactly at the arrival time of the wave with the minimum group velocity, namely $U_{min}=0.9194\,V_s$.

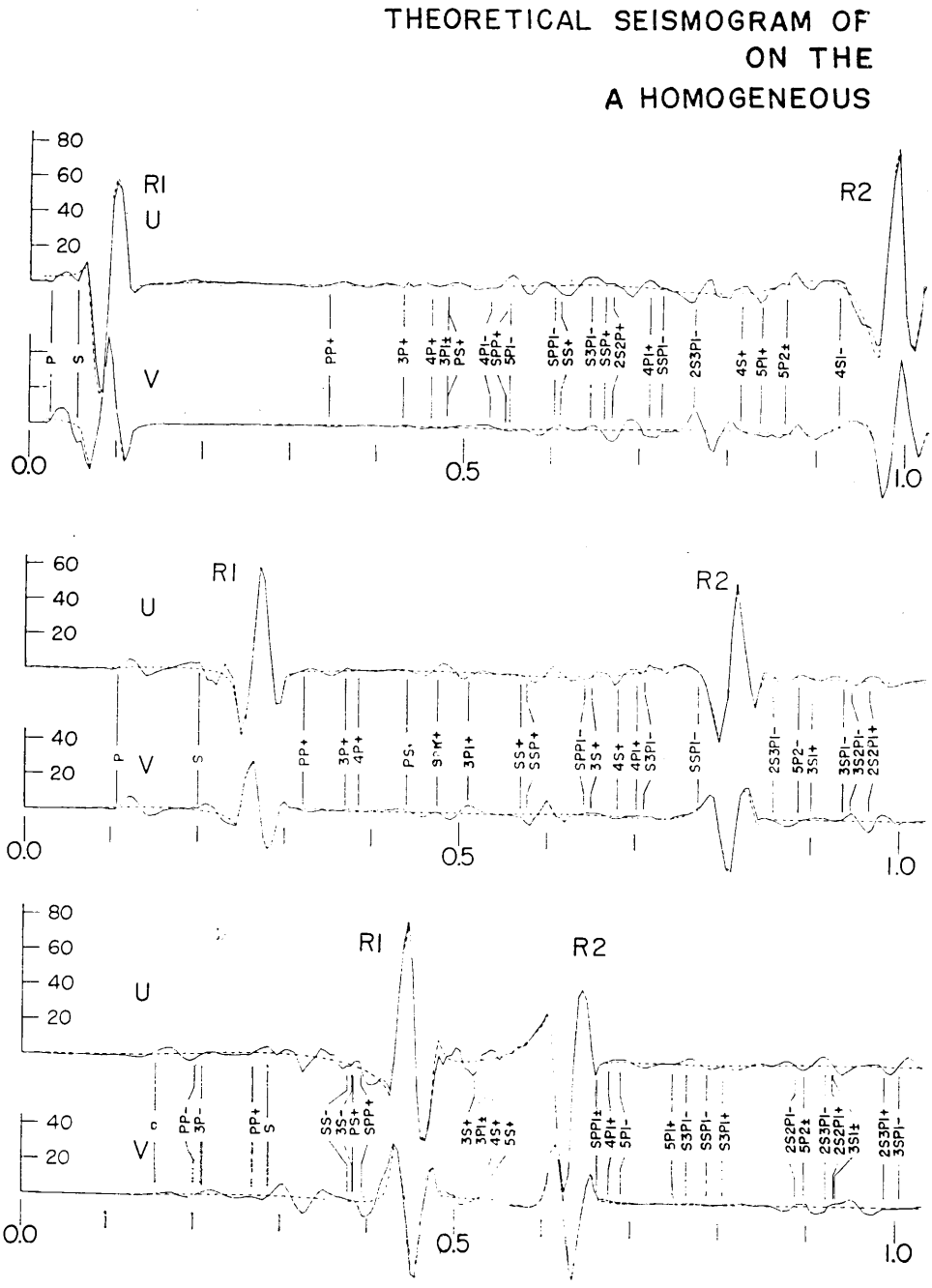

Fig. 4. Theoretical seismograms of radial and colatitudinal a localized radial stress around the pole. Arrows show the theory of geometrical optics. Solid line: $({}_9u_{100})$ and $({}_9v_{100})$. Broken are the radius and shear velocity of the sphere. $nPmS$ implies the end of notation means the epicentral distance to be $2(k+1)\pi-\theta$

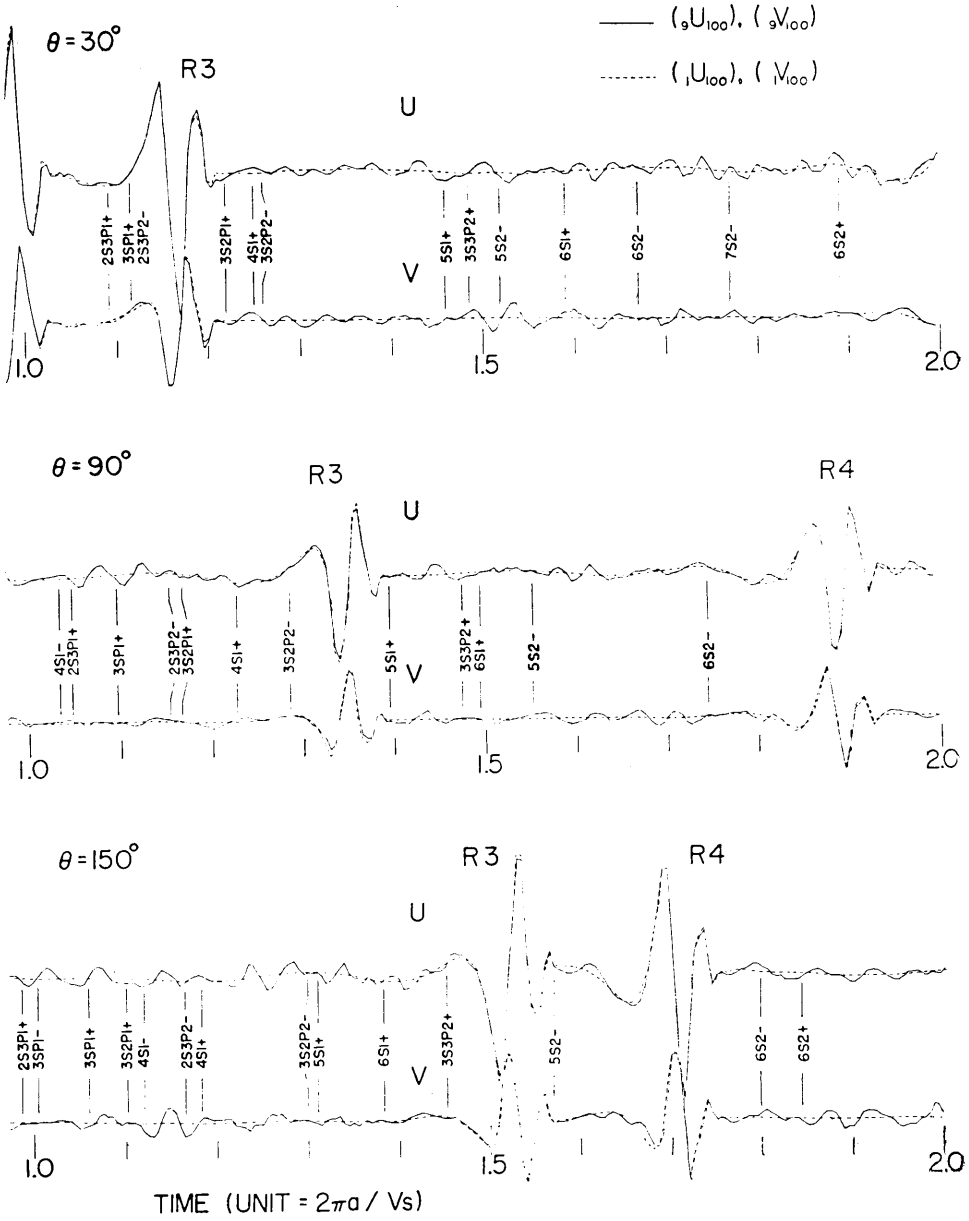

displacement at epicentral distances $\theta=30°$, 90° and 150° due to arrivals of various phases of body waves calculated by a simple line: ($_1u_{100}$) and ($_1v_{100}$). Unit of time is $2\pi a/V_s$, where a and V_s *PP—PPSS—SS*, *P* being n times and *S* being m times. $k+$ in and $k-$ means the epicentral distance to be $2k\pi \pm \theta$.

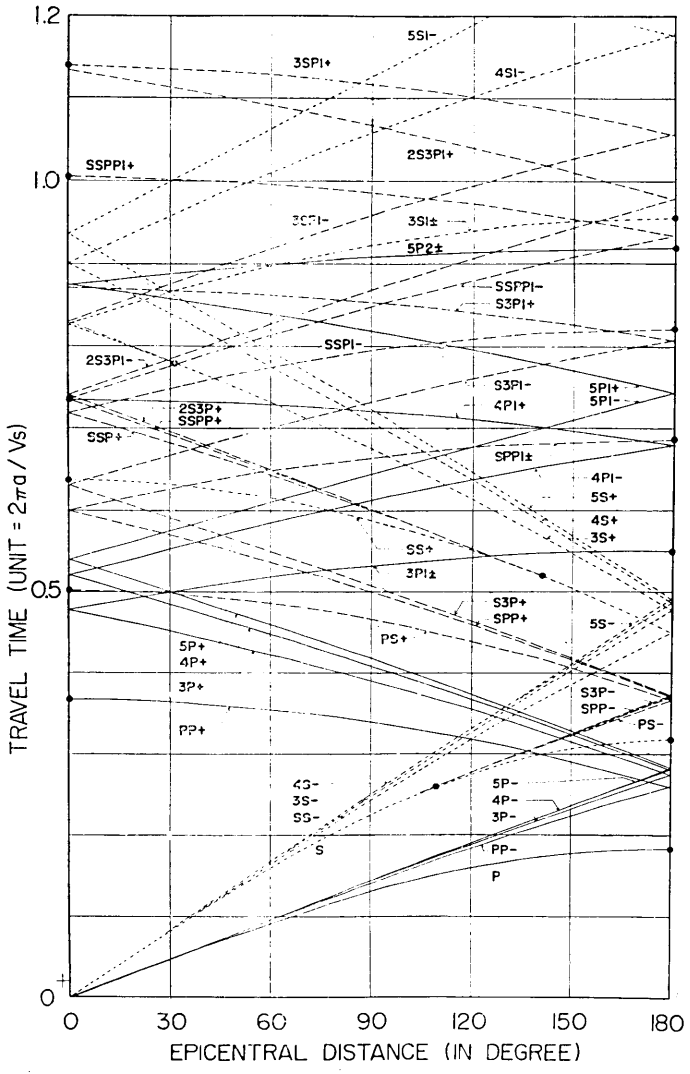

Fig. 5. Travel time curves of various body waves for a point source at the pole. Cross mark on the lower left is the reference point in the present case. Solid line: P wave. Broken line: S wave. Chain line: P-S converted wave. Dots show the beginning point of SnP, $SSnP$ and $3SnP$ waves, n being an integer. Those on the ordinate at epicentral distances 0° and 180° are end points of various phases.

7. Phase velocity obtained by the method of Fourier transform

Phase velocity calculated by the method of Fourier transform[6] using the theoretical seismogram is shown in Figs. 6a, 6b, 6c and 6d. It shows a good agreement with the curve determined by the formula (4.3). Figs. 6c and 6d show the phase velocity of the first higher mode ($i=2$) calculated by the same method. The data is $({}_2u_{100})-({}_1u_{100})$, which is the contribution of only the first higher mode. The curve is given in Fig. 7.

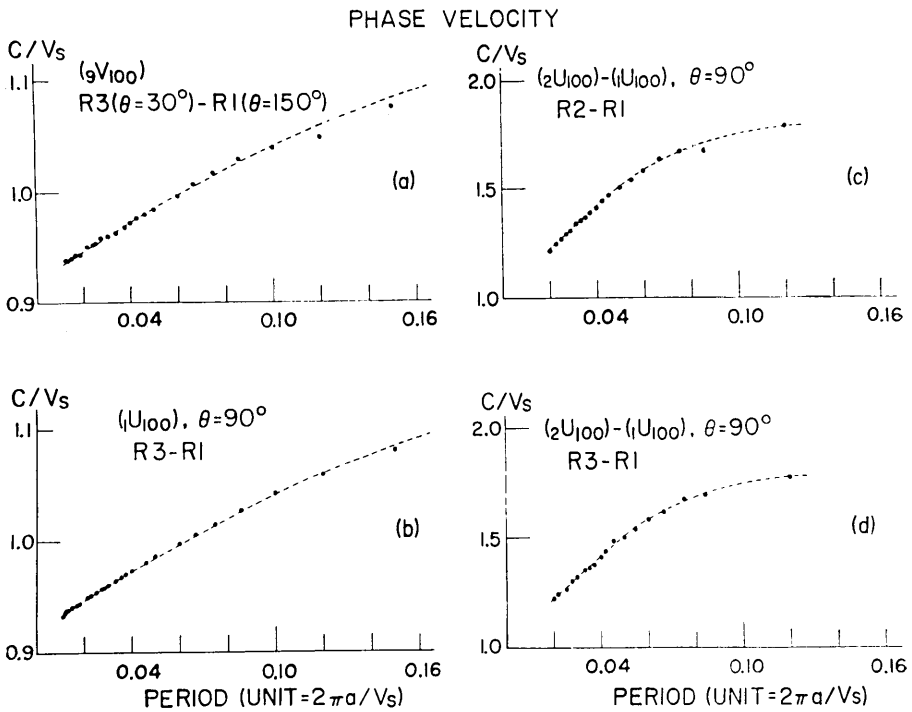

Fig. 6. Comparison of phase velocity calculated from Fourier transform method (dots) with those computed from non-dimensional frequency by the equation (4.3), (broken line). (a) and (b) are for the fundamental mode ($i=1$) and (c) and (d) for the first higher mode ($i=2$).

Acknowledgments

Our thanks go to Watson Research Laboratory, IBM, New York for giving us the advantage of commencing this study using computation

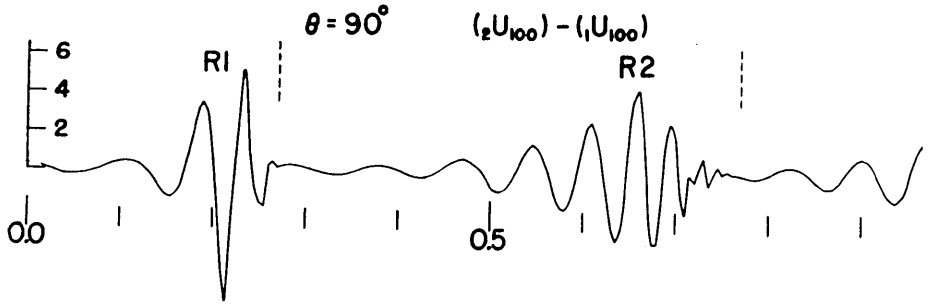

Fig. 7. Radial disturbance at $\theta=90°$ for $i=2$, which is the contribution of only the mode (Fig. 4, broken line). Parts of the seismogram employed for the numerical work minimum group velocity for $i=2$.

facilities. The numerical work was carried out by an IBM 7090 through the courtesy of IBM, Japan Ltd. and the Computation Centre, the University of Tokyo, to which our sincere thanks are due.

During his stay at Lamont, Dr. Usami was supported through Air Force Cambridge Research Laboratories under contract AF19 (604) 7376 as part of Project VELA, sponsored by the Advanced Research Projects Agency.

References

1) Y. SATÔ, T. USAMI and M. EWING (1962), "Basic Study on the Oscillation of a Homogeneous Elastic Sphere IV. Propagation of Disturbances on the Sphere." *Geophys. Mag.* **31**, pp. 237-242.
Y. SATÔ, T. USAMI, M. LANDISMAN and M. EWING (1963), "Basic Study on the Oscillation of a Sphere Part V: Propagation of Torsional Disturbances on a Radially Heterogeneous Sphere. Case of a Homogeneous Mantle with a Liquid Core." *Geophys. J.* **8**, pp. 44-63.
2) Y. SATÔ and T. USAMI (1962), "Basic Study on the Oscillation of a Homogeneous Elastic Sphere I. Frequency of the Free Oscillations." *Geophys. Mag.*, **31**, pp. 15-24.
3) T. MATUMOTO and Y. SATÔ (1954), "On the Vibration of an Elastic Globe with One Layer. Vibration of the First Class." *Bull. Earthq. Res. Inst.*, **32**, pp. 247-258.
4) *loc. cit.* first paper of 1).
5) *loc. cit.* 1).
6) Y. SATÔ (1955), "Analysis of Dispersed Surface Waves by means of Fourier Transform I." *Bull. Earthq. Res. Inst.*, **33**, pp. 33-48.

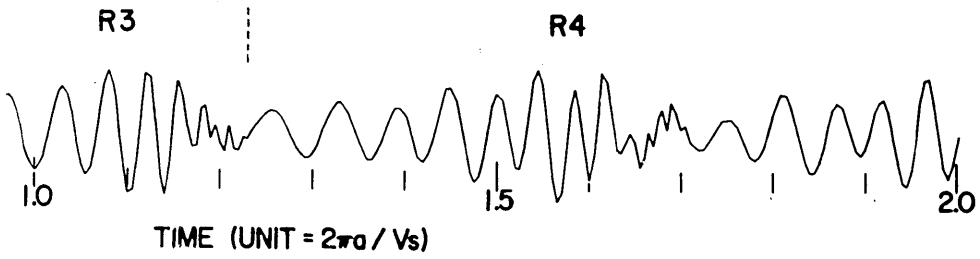

first higher mode, which shows more dispersive character than that of the fundamental are shown by R1, R2 and R3 which end abruptly at the arrival time of waves with

15. 等方等質弾性球の表面を伝わるスフェロイド型の振動

地震研究所 宇佐美 龍 夫
佐 藤 泰 夫

1. 筆者らはさきに，弾性球を伝わる捩れ波を球のいろいろなモードの固有捩れ振動の和として表わし，実際の地震によく似た理論地震記象を求めた．今回は同様な方法を用い，等方等質弾性球の極附近に半径方向の力が加わる場合の変位を，球面上の数点で計算した．

2. 理論地震記象をより精度の高いものとするために，筆者らが前に求めた固有振動数に，$i=6\sim9$, $n\geqq0$; $i=1\sim5$, $n>60$ に対する固有振動数を追加計算した．ついでこれから，位相速度と群速度を求めた．群速度に極大，極小が表われたが，これは捩れ波の場合と著しく異なる点である．また，波長が小さくなると，位相速度も群速度も等方等質半無限弾性体のレイリー波の速度 ($0.9194\times S$ 波速度) に近ずく．さらに，スペクトルのうち観測点と時刻に無関係な部分をコモンスペクトルと呼び，これを図に示してある．

3. 実際の計算にあたつては，軸対称 ($m=0$) を仮定し，また，力の空間的分布 $\Phi(\theta,\varphi)$，時間的分布 $f(t)$ を次のようにとつた．

$$\Phi(\theta,\varphi)=\begin{cases}1 & \theta\leqq\theta_0\,,\\ 0 & \theta>\theta_0\,.\end{cases}\qquad(\theta_0=0.04\ \text{ラヂアン})$$

$$f(t)=\begin{cases}-1 & -t_1<t<0\,,\\ 1 & 0<t<t_1\,,\\ 0 & t_1<|t|\,.\end{cases}\qquad(t_1=0.02)$$

時間の単位は，(周長)/(S 波の速度) である．(S 波速度を 6.67 km/sec, 球の半径 6370 km とすると，この値はほぼ 100 分となる.) 変位は，時間 $t=0.0\,(0.005)\,2.0$ について計算し，その結果次の事が明らかになつた．

a) 幾何光学的な考えから求められた実体波の走時は，理論地震記象の中に見られる各波の発現時刻とよく一致する．

b) 基本振動は表面波を表わし，また逆に表面波は基本振動によつて表わされる．高次の ($i\geqq2$) 振動は実体波と密接に関係し，表面波との関係は少ない．球の問題で，表面波分散曲線の高次の分枝の持つ意義は興味深い．

c) 群速度に極小値がある事に対応し，表面波の終りの点がはつきりと理論記象上に見出される．その時刻は震央距離を極小群速度でわつて得られる走時と一致する．

4. 理論記象を与えられたものとして，フーリエ解析の方法により，位相速度を求めた．これは先に振動数 ((4.3) 式) から求めたものとよく一致する．なお，第一次の高調波 ($i=2$) による変位のみをとりだし，同じように解析した結果も図に示す．